Enhanced chemotherapy response in hepatocellular carcinoma: synergistic effects of miR-122 and doxorubicin co-delivery system inducing apoptosis and DNA damage

Xiuyun Lin[1], Jie Liu[1], Guangfeng Wu[1], Xiu Yang[1], Wenqiang Yan[2], Nanfeng Fan[1] and Hui Li[1*]

*Correspondence:
lihui770105@126.com

[1] Department
of Hepatopancreatobiliary
Medical Oncology, Clinical
Oncology School of Fujian
Medical University, Fujian Cancer
Hospital, Fuzhou, Fujian, People's
Republic of China
[2] Department of Pharmacy,
Fujian Medical University Union
Hospital, Fuzhou, Fujian, People's
Republic of China

Abstract

Background: Cancer cells can resist chemotherapy through various mechanisms, diminishing treatment outcomes. Research had indicated that combining miR-122 with doxorubicin (DOX) can improve hepatocellular carcinoma (HCC) therapy.

Results: To explore this, we created a one-pot co-delivery system, Fe-miR-122/DOX, by coordinating miR-122, DOX, and Fe^{II} ions into nanoparticles. These nanoparticles display uniform particle sizes, well-defined morphology, and exceptional colloidal stability in 10% FBS and 20% FBS solution over 24 h. When the ratio of DOX to miR-122 was set at 20:1, the loading efficiency of both drugs reached 54.7% and 55.5%, respectively. Cell experiments confirmed that Fe-miR-122/DOX efficiently delivers both miR-122 and DOX, enabling cytoplasmic delivery through lysosomal escape, facilitated by the positive charge of the nanoparticles. Functionally, miR-122 increases intracellular accumulation of DOX by downregulating P-glycoprotein (P-gp) expression, and it promotes apoptosis by downregulating B-cell lymphoma 2 (Bcl-2), which leads to the upregulation of Caspase-3. Additionally, Fe-miR-122/DOX disrupts cIAPs-mediated anti-apoptotic signals, downregulates PARP-1 expression, hinders DNA repair, promotes DNA fragmentation, enhances caspase-3 expression, and triggers programmed cell death, synergistically enhancing its antitumor efficacy. This synergistic mechanism disrupts DNA repair, amplifying DNA damage and apoptosis. Our cytotoxicity and apoptosis assays (with a HepG2 cell apoptosis rate of 85.98%) demonstrated the potent antitumor capability of Fe-miR-122/DOX.

Conclusions: This innovative system has demonstrated good biocompatibility and has the potential to transform HCC therapy. Future research could focus on optimizing the co-delivery system and assessing its efficacy in clinical trials.

Keywords: Chemotherapy resistance, miR-122, Hepatocellular carcinoma (HCC), Nanoparticles, Apoptosis

Lin *et al. Cancer Nanotechnology* (2024) 15:48

Page 2 of 15

Introduction

Hepatocellular carcinoma (HCC) is a significant global health burden, ranking seventh in cancer prevalence and fourth in cancer-related mortality (Bray et al. 2018). Despite the availability of surgical interventions like radiofrequency ablation, hepatectomy, and liver transplantation as primary treatment modalities (Vogel et al. 2022; Yarchoan et al. 2019), late diagnosis often leads to missed surgical opportunities, resulting in high recurrence rates and poor long-term outcomes (Lee et al. 2018). Consequently, non-surgical therapies, particularly chemotherapy, retain significant importance in the treatment landscape of HCC. However, conventional chemotherapeutic agents encounter challenges such as hydrophobicity, poor tumor specificity, short circulation times, and significant toxicity to normal tissues, limiting their efficacy (Yingchoncharoen et al. 2016). Furthermore, patient resistance to common chemotherapeutic agents like cisplatin, 5-fluorouracil, doxorubicin, and mitomycin poses further complications, emphasizing the urgent need to enhance chemotherapy effectiveness (Li et al. 2023; Takai Takamatsu et al. 2019; Wang et al. 2021a, b).

MicroRNAs (miRNAs), a family of small, non-coding RNAs, play pivotal roles in cancer pathogenesis, progression, and prognosis. Among them, miR-122, accounting for approximately 70% of the hepatic miRNA repertoire, is frequently downregulated in HCC and closely associated with disease progression and metastasis (Bracken et al. 2016; Nakao et al. 2014). Research indicates that miR-122 exerts tumor-suppressive functions in HCC by promoting apoptosis and inhibiting cellular proliferation (Rupaimoole and Slack 2017; Xu et al. 2012). Moreover, upregulation of miR-122 enhances the sensitivity of HCC cells to multiple chemotherapeutic agents, suggesting its potential as a therapeutic adjunct. Nevertheless, integrating miR-122 with conventional chemotherapy faces challenges due to differences in physical and chemical properties (Cao and Yin 2019; Fornari et al. 2009; Xu et al. 2011). Additionally, practical application of miRNA is hindered by low transfection efficiency and instability, necessitating suitable delivery systems (Xiong et al. 2021a, b). Various drug carriers, such as liposomes (Mendes et al. 2022) and inorganic nanoparticles (Li et al. 2022), have been developed to address these issues but are limited by their complex designs and specialized preparation processes.

To overcome these challenges, we synthesized the Fe-miR-122/DOX nanoparticle by integrating miR-122, doxorubicin (DOX), and Fe^{II} ions based on the previously reported coordination-driven self-assembly approach (Scheme 1a) (Li et al. 2018; Zou et al. 2021). This advanced system features precise morphology, exceptional colloidal stability, and high drug loading efficiency. Crucially, the positively charged Fe-miR-122/DOX nanoparticles promote lysosomal escape, thereby facilitating cytoplasmic drug release and enhancing chemotherapy efficacy. Upon escaping lysosomal degradation, miR-122 and DOX synergistically exert anticancer activity. miR-122 increases intracellular accumulation of DOX by downregulating P-glycoprotein (P-gp) expression, and it promotes apoptosis by downregulating B-cell lymphoma 2 (Bcl-2), which leads to the upregulation of Caspase-3. Elevated DOX levels in cells result in increased DNA damage, further stimulating apoptosis. Furthermore, Fe-miR-122/DOX not only effectively suppresses cIAPs-mediated anti-apoptotic signaling, but also significantly reduces PARP-1 expression, thereby disrupting DNA repair mechanisms and promoting the accumulation of DNA fragmentations (Scheme 1b). Through these mechanisms, Fe-miR-122/DOX disrupts

Lin *et al. Cancer Nanotechnology* (2024) 15:48

Page 3 of 15
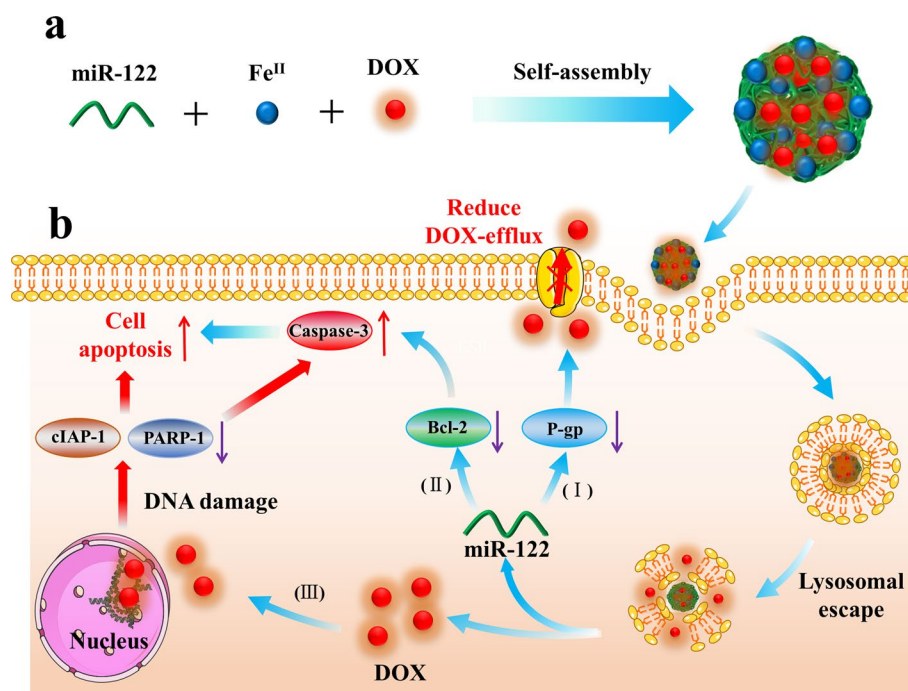
Scheme 1 **a** Schematically illustrates the Fe-miR-122/DOX nanocomplex assembly through a Fe^{II}-ion-driven coordination process involving DOX and DNA molecules. **b** The therapeutic mechanism of the Fe-miR-122/DOX complex in HCC is elucidated: upon HepG2 cell uptake, the complex escapes the endosome, releasing miR-122 and DOX into the cytosol. MiR-122 exerts dual actions; it downregulates P-glycoprotein (P-gp) (I), reducing extracellular efflux of doxorubicin, while inhibiting Bcl-2 expression (II), thereby enhancing caspase-3 expression to promote apoptosis. Simultaneously, DOX translocates to the nucleus (III), effectively inhibiting cIAPs-mediated anti-apoptotic signaling, reducing PARP-1 expression, inducing DNA damage, ultimately yielding a synergistic antitumor effect

DNA repair processes and amplifies DNA fragmentation, leading to enhanced cell apoptosis. Experimental evidence of cytotoxicity and cell apoptosis confirms the superior antitumor ability of this nanocomplex, highlighting its significant therapeutic potential in improving liver cancer treatment outcomes.

Experimental details and methods

Chemicals and materials

All chemicals were of analytical grade and used as received without further purification. Doxorubicin hydrochloride (DOX) and ferric chloride tetrahydrate ($FeCl_2 \cdot 4H_2O$) were purchased from Aladdin. Hoechst 33342 was obtained from Solarbio (Beijing, China). Lyso Tracker Deep Red was purchased from Sigma-Aldrich (USA). Cell Counting Kit-8 (CCK-8) and Annexin V-FITC Apoptosis Detection Kit were purchased from BestBio (Shanghai, China). DNA was sourced from Sangon Biotech (Shanghai, China). All solutions were prepared using ultrapure water from a Milli-Q purification system (resistance of 18.2 MΩ). P-Glycoprotein, Bcl-2, RAPR-1, cIAP1 and Caspase-3 antibodies and corresponding secondary antibodies were obtained from Abcam.

Lin *et al. Cancer Nanotechnology* (2024) 15:48

Page 4 of 15

General measurements

The scanning electron microscopy (SEM) images were acquired using a Thermo Scientific Verios G4 UC system, while transmission electron microscopy (TEM) images were obtained with an HT7700 transmission electron microscope (HITACHI, Japan) operating at 100 kV. Zeta-potential and Dynamic Light Scattering (DLS) measurements were conducted with a Malvern Zetasizer Nano ZS instrument (Malvern, UK). Fluorescence spectra were recorded using a Cary Eclipse Fluorescence Spectrophotometer (Agilent Technologies, Australia). Fluorescence cellular imaging was performed using a confocal laser scanning microscope (CLSM, Nikon A1+, Japan). Flow cytometric analysis was carried out utilizing a BD FACS CantoTM II Flow Cytometer.

Preparation of Fe-miR122/DOX nanospheres

Mix 15 µL of miR-122 (100 µM) with 6 µL of DOX solution (5 mM) and dilute with distilled water to a total volume of 70 µL. Vortex the mixture quickly to ensure everything is well mixed. Then, add 30 µL of $FeCl_2 \cdot 4H_2O$ (1 mM) and vortex again. Heat the final mixture to 95 °C and keep it at that temperature for 1 h. Let it cool naturally, then centrifuge the Fe-miR122/DOX mixture at 13,000 rpm for 15 min and wash with distilled water. Redisperse the Fe-miR122/DOX in 100 µL of methanol and store for future use.

Loading calculation and release

The supernatant and wash solutions were collected to evaluate the loading efficiency of DOX and miR122 in Fe-miR122/DOX. Fluorescence spectroscopy was used to measure the unloaded DOX and miR122-Cy5, while Fe was determined by ICP-MS. For the drug release experiments, the obtained Fe-miR122/DOX was immersed in HEPES buffer or cell lysates solution at 37 °C with gentle shaking. At predetermined time intervals, the supernatant was collected by centrifugation and replaced with an equal volume of fresh HEPES. The release amount of DOX and miR122-Cy5 at specific times was determined by measuring the fluorescence intensity in the supernatant. The calculation formulas for drug loading content (DLC) and encapsulation efficiency (DLE) are as follows: DLC (%) = (weight of loaded DOX/total weight of Fe-miR122/DOX) × 100%, DLE (%) = (weight of loaded DOX/total weight of DOX) × 100%.

Cellular uptake assay

HepG2 cells (2×10^4 cells per well) were seeded in confocal culture dishes (Corning) and treated with PBS, miR-122-Cy5, DOX, Fe-miR-NC-Cy5/DOX, or Fe-miR122-Cy5/DOX nanoparticles (final concentrations of [DOX] = 50 µg mL^{-1}, [miR-122] = 270 nmol L^{-1}) for 2, 4, 6, or 12 h. Subsequently, the cells were washed three times with PBS to remove non-internalized materials. Cell uptake was then analyzed through CLSM imaging.

Intracellular lysosome localization

HepG2 cells (2×10^4 cells per well) were seeded in confocal culture dishes (Corning) and treated with Fe-miR-122/DOX or Fe-miR-NC/DOX nanoparticles (final concentrations of [DOX] = 50 µg mL^{-1}, [miR-122] = 270 nmol L^{-1}) for 2, 4, 6, or 12 h. Following the manufacturer's protocol, cells were stained with Lysotracker Red and Hoechst 33,342 for lysosomes and cell nuclei, respectively. After washing the cells with PBS, CLSM was

Lin *et al. Cancer Nanotechnology* (2024) 15:48

Page 5 of 15

used to observe the co-localization. Hoechst 33,342, FITC, and Lysotracker Red were excited at 405, 488, and 640 nm, respectively.

Cell toxicity assay

HepG2 cells were used as the study model, and cell toxicity was assessed using the CCK-8 assay. HepG2 cells were seeded at a density of 1×10^4 cells per well in a 96-well plate and cultured in DMEM medium containing 15% (FBS and 1% penicillin–streptomycin, 37 °C, 5% CO_2) for 12 h. Subsequently, PBS, miR-122, DOX, Fe-miR-NC/DOX, or Fe-miR122/DOX nanoparticles (final concentrations of [DOX] = 50 μg mL^{-1}, [miR-122] = 270 nmol L^{-1}) were added to the wells. After incubation for 24 h, the culture medium was removed, and 100 μL of fresh medium containing 10% (v/v) CCK-8 was added to each well and further incubated for 1 h. The absorbance value at 450 nm was measured by microplate reader and the cytotoxicity was calculated.

Huh-7 or L02 cells were used as the study model, and cell toxicity was assessed using the CCK-8 assay. Huh-7 or L02 cells were seeded at a density of 1×10^4 cells per well in a 96-well plate and cultured in 1640 medium containing 10% (FBS and 1% penicillin–streptomycin, 37 °C, 5% CO_2) for 12 h. Subsequently, Fe-miR122/DOX nanoparticles (final concentrations of [DOX] = 50 μg mL^{-1}, [miR-122] = 270 nmol L^{-1}) was added to the wells. After incubation for 24 h, the culture medium was removed, and 100 μL of fresh medium containing 10% (v/v) CCK-8 was added to each well and further incubated for 1 h. The absorbance value at 450 nm was measured by microplate reader and the cytotoxicity was calculated.

Apoptosis assay

To investigate apoptosis in HepG2 cells, 1×10^6 cells were seeded in 6-well plates. After 24 h, the cells were treated with PBS, miR-122-Cy5, DOX, Fe-miR-NC-Cy5/DOX, or Fe-miR122-Cy5/DOX nanoparticles (final concentrations of [DOX] = 50 μg mL^{-1}, [miR-122] = 270 nmol L^{-1}). Following the incubation period, the supernatant was collected, and the adherent cells were detached using trypsin and collected. The cells collected after centrifugation of the supernatant and those collected after digestion were washed with PBS buffer. The cells were then stained using a cell apoptosis analysis kit containing Annexin V-FITC and propidium iodide (PI) according to the manufacturer's instructions. Cell apoptosis was evaluated using a BD FACS CantoTM II Flow Cytometer.

Western blotting

HepG2 cells (2×10^5 per well) were seeded in 6-well culture plates and incubated for 12 h. The cells were washed three times with PBS and further incubated with PBS, miR-122-Cy5, DOX, Fe-miR-NC-Cy5/DOX, or Fe-miR122-Cy5/DOX nanoparticles (final concentrations of [DOX] = 50 μg mL^{-1}, [miR-122] = 270 nmol L^{-1}). Protein was collected using RIPA lysis buffer, and total protein quantification was performed using a BCA protein assay kit. Twenty micrograms of protein extracts were separated by 10% SDS-PAGE and transferred to a PVDF membrane. The membrane was then incubated overnight with monoclonal antibodies against P-glycoprotein, Bcl-2, RAPR-1, cIAP1, Caspase-3, and β-actin (used as an internal control). After washing, the membrane was incubated with HRP-conjugated secondary antibodies at room temperature for

Lin *et al. Cancer Nanotechnology* (2024) 15:48

Page 6 of 15

1 h. Bands were detected using chemiluminescent substrate (SuperSignal West Pico, Thermo) and imaged with a gel imaging system. Western blot quantification was performed using ImageJ software, and heat maps were generated using GraphPad Prism software for visualization.

Results and discussion

Synthesis and characterization of Fe-miR-122/DOX

By meticulously combining miR-122, DOX, and Fe^{II} ions in aqueous solution at a specific molar ratio (1:20:20) and incubating at 95 °C for 1 h, we successfully synthesized Fe-miR-122/DOX nanoparticles. Representative transmission electron microscopy (TEM) and scanning electron microscopy (SEM) images depict uniform spherical morphology and smooth surface features (Fig. 1a and b). Dynamic light scattering (DLS) measurements revealed an average diameter of approximately 155.6 nm for Fe-miR-122/DOX (Additional file 1: Fig. S1), along with a Zeta-potential of approximately + 3.79 mv (Fig. 1c). The formation process of the Fe-miR-122/DOX nanoparticles resembles those observed in metal–organic frameworks (MOFs), which can be elucidated through the LaMer model (Wang et al. 2018). This model delineates rapid nucleation followed by uniform growth into consistent-sized particles. Time-dependent TEM analysis confirmed nucleation completion within 15 min, and as the reaction time increases, the nanoparticles gradually increase in size (Additional file 1: Figs. S2 and S3). Furthermore, UV–visible absorption spectroscopy confirms the successful incorporation of miR-122 and DOX into the Fe-miR-122/DOX nanoparticles (Additional file 1: Fig. S4).

Notably, the methodology employed facilitates ultra-efficient and precisely controlled encapsulation of miR-122 and DOX. Varying molar ratios of DOX to miR-122 (5:1, 10:1, 15:1, and 20:1) during nanoparticle synthesis yielded nanoparticles with good sphericity and uniformity in size (Additional file 1: Fig. S5). Increasing the DOX to miR-122 molar ratio from 5:1 to 20:1 enhanced DOX loading content (DLC) from 24.48 wt% to 58.35 wt%, while miR-122 declined from 64.91 wt% to 34.03 wt% (Fig. 1d and Additional file 1:
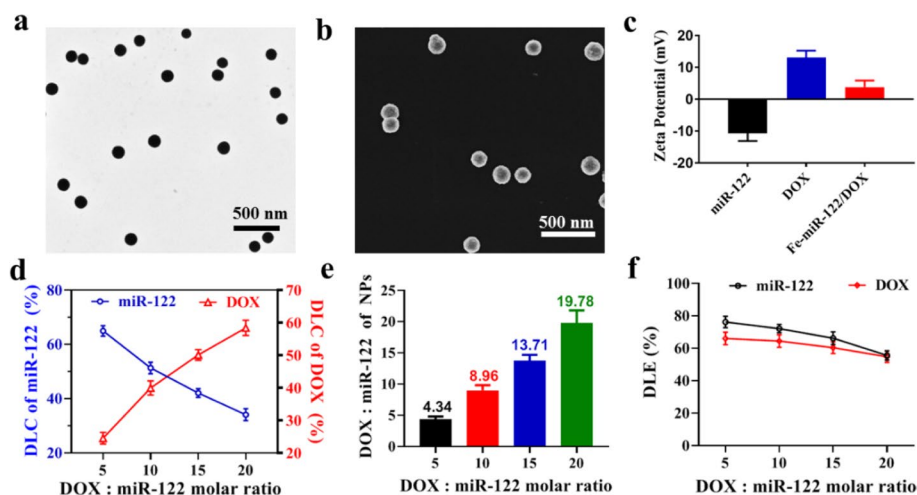

Fig. 1 **a** TEM image and **b** SEM image of Fe-miR-122/DOX. **c** Zeta-potentials of miR122, DOX and Fe-miR-122/DOX. **d** DLC of miR122 (blue line) and DOX (red line), **e** the DOX: miR122 molar ratios, and **f** DLE of DOX and miR122 in the NPs with different added ratios of DOX:miR122 in the synthesis (n = 3)

Lin *et al. Cancer Nanotechnology* (2024) 15:48

Page 7 of 15

Figs. S6-7). Fine-tuning the DOX to miR-122 ratio (4.34 to 19.78) within the nanoparticles is achievable by adjusting the initial ratio during preparation (Fig. 1e). Furthermore, when the initial molar ratio of DOX to miR-122 is below 10.0, both the DOX and miR-122 display drug loading efficiency (DLE) exceeding 70% (Fig. 1f). Such high DLC and DLE significantly surpass those of traditional nano-carrier delivery systems, attributed to the dual role of DOX and miR-122—serving not only as therapeutic agents, but also participating in the assembly of nanoparticles through cooperative interactions. According to the Chou–Talalay method, the combination index (CI) for DOX and miR-122 at 10:1, 15:1, 20:1, 30:1 and 40:1 ratios was found to be less than 1, indicating synergistic therapeutic effects (Additional file 1: Fig. S8). Literature also had supported that a DOX to miR-122 ratio greater than 10:1 yields synergistic outcomes (Zhang et al. 2021). However, when the DOX ratio exceeds 20, the nanoparticles tend to precipitate in solution, likely due to the hydrophobic nature of DOX. Therefore, given the enhanced drug loading content and efficiency observed at higher ratios, we selected the 20:1 ratio for further experiments to maximize therapeutic payload delivery and nanoparticle stability.

Stability and responsiveness of Fe-miR-122/DOX

Considering the non-covalent nature of coordination-driven self-assembly, stability of nanoparticles plays a crucial role in delivery systems. To investigate this, we examined the stability of Fe-miR-122/DOX nanoparticles (with a DOX to miR122 molar ratio of 20:1). TEM and DLS results revealed that the Fe-miR-122/DOX nanoparticles remained intact for 24 h in both water and HEPES buffer solution, but showed significant degradation by 48 h (Fig. 2a and Additional file 1: Fig. S9). However, when placed in 10% and 20% FBS, the Fe-miR-122/DOX nanoparticles maintained good monodispersity and spherical morphology for 24 h. Although partial disintegration was observed at 48 h, some of the nanoparticle structure was still discernible (Fig. 2a). This enhanced stability
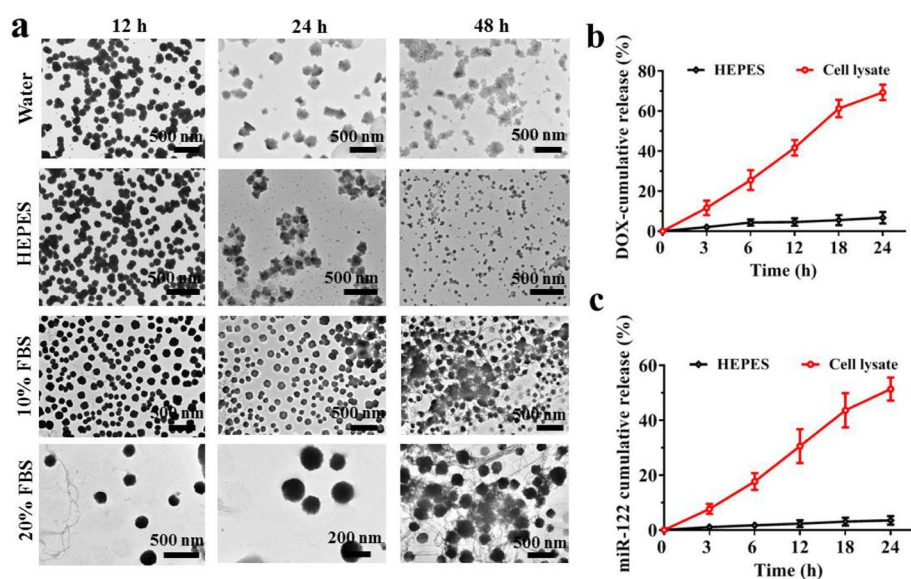

Fig. 2 a TEM images of Fe-miR-122/DOX incubated in water, HEPES, 10%FBS and 20%PBS for 12 h, 24 h and 48 h, respectively. **b** and **c** The cumulative release of miR122 and DOX for Fe-miR-122/DOX in cell lysate (n = 3)

Lin *et al. Cancer Nanotechnology*   (2024) 15:48

Page 8 of 15

can be attributed to the adsorption of proteins by the positively charged nanoparticles, forming a protective protein corona that modulates ionic strength and osmotic pressure, thereby reducing surface energy and preventing aggregation. Additionally, FBS buffers the pH of the solution, providing a more stable environment that further enhances nanoparticle stability.

Furthermore, we assessed the drug release kinetics of Fe-miR-122/DOX nanoparticles under in vitro conditions. In HEPES buffer solution, the release of DOX and miR-122 was only 7.6% and 3.5%, respectively, over a 24-h period. However, upon exposure to cell lysate, the release profiles of both drugs showed a time-dependent increase, with Fe-miR-122/DOX nanoparticles exhibiting a release rate of 70.3% for DOX and 51.4% for miR-122 within 24 h, indicating a high responsiveness to the cellular environment (Fig. 2b and c). This release behavior is primarily attributed to the self-assembly process of Fe-miR-122/DOX nanoparticles, which relies on electrostatic attraction and coordination between Fe^{II} ions and miR-122, as well as π-π stacking interactions between miR-122 and DOX. Under HEPES buffer solution, Fe^{II} ions form stable complexes with the phosphate groups of miR-122, maintain stability of the nanoparticles. Concurrently, the aromatic rings of miR-122 further interact with those of DOX through π–π stacking, enhancing nanoparticle stability. Upon cell lysate environment, such as changes pH or the presence of reducing agents can disrupt the Fe^{II}-miR-122 interactions, leading to DOX release. Additionally, enzymatic activity, interactions with cellular components, and variations in temperature and ionic strength collectively facilitate efficient drug release.

Fe-miR-122/DOX nanoparticles uptake and lysosomal escape

To investigate the uptake of Fe-miR-122/DOX nanoparticles by HCC cells (HepG2), we labeled miRNA-122 with Cy5 and conducted imaging analysis using confocal laser scanning microscopy (CLSM). Additionally, we synthesized a control nanoparticle using an arbitrary miRNA sequence (miR-NC) employing the same method as Fe-miR-122/DOX, confirming the method's versatility across various miRNA sequences (Additional file 1: Fig. S10). HepG2 cells were incubated with Fe-miR-122/DOX and control formulations (PBS, miR-122, DOX, and Fe-miR-NC/DOX) for 2, 4, 6, and 12 h before CLSM examination. HepG2 cells were exposed to Fe-miR-122/DOX and control formulations (PBS, miR-122, DOX, and Fe-miR-NC/DOX) for 2, 4, 6, and 12 h before CLSM examination. Our results indicated higher Cy5 and DOX fluorescence intensities in the nanoparticle-treated groups compared to controls after 2 h, signifying enhanced nanoparticle internalization (Fig. 3 and Additional file 1: Figs. S11-S12). The fluorescence intensity peaked at 4 h, indicating maximal cellular uptake at this juncture, with gradual decreases in Cy5 and DOX fluorescence over extended incubation periods, potentially due to cellular exocytosis of nanoparticles. Notably, consistent co-localization analysis of DOX and Cy5 fluorescence signals, supported by Pearson's correlation coefficient, highlighted the Fe-miR-122/DOX nanoparticles' ability to concurrently deliver DOX and miR-122 (Additional file 1: Fig. S13). The rapid cellular uptake observed, coupled with its dual drug delivery potential, holds promise for enhancing combinatorial cancer treatment efficacy.

To further explore the intracellular distribution of Fe-miR-122/DOX, lysosomal quantitative analysis techniques were employed to assess Fe-miR-122/DOX (green, DOX)
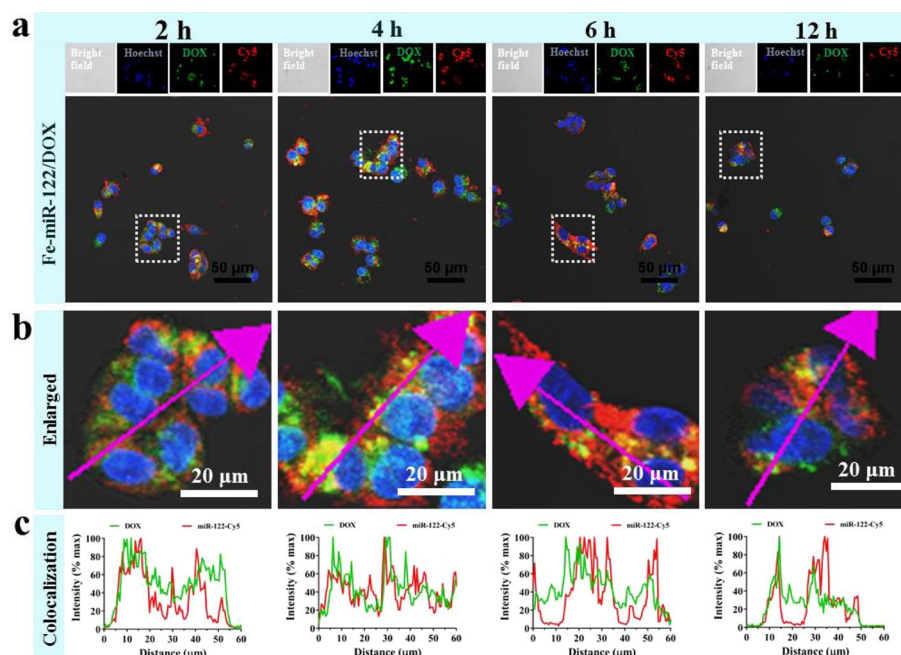
Lin *et al. Cancer Nanotechnology* (2024) 15:48

Page 9 of 15

Fig. 3 a CLSM images of HepG2 cells treated with Fe-miR122-Cy5/DOX for different time. **b** and **c** Fluorescent intensity of DOX and miR122-Cy5 signals across 60-μm regions marked with arrows is shown in line plots

co-localization with lysosomes (red, LysoTracker) in vitro. Following a 2 h co-incubation with HepG2 cells, pronounced co-localization between DOX and lysosomes indicated successful Fe-miR-122/DOX transport into lysosomes. However, as incubation time progressed from 4 to 12 h, a gradual separation of green and red fluorescence emerged, suggesting Fe-miR-122/DOX escape from lysosomes (Fig. 4). This lack of co-localization was further supported by a Pearson correlation coefficient of 0.467 (Additional file 1: Fig. S14), below the typical co-localization threshold, likely attributed to electrostatic disruption of lysosomal membranes by positively charged nanoparticles, facilitating lysosomal escape (Agirre et al. 2014; Wang et al. 2021a, b). These findings suggested effective Fe-miR-122/DOX nanoparticle internalization by HepG2 cells and confirmed their ability to synergistically deliver drugs within cells and facilitate lysosomal escape.

Cytotoxicity evaluation of Fe-miR-122/DOX nanoparticles in liver cancer cells

Subsequently, we evaluated their cytotoxic effects on HepG2 cells using the Cell Counting Kit-8 (CCK-8) assay (Fig. 5a). While the PBS and miR122 groups showed minimal cytotoxicity, both DOX and Fe-miR-NC/DOX groups exhibited concentration-dependent cytotoxicity. Notably, the Fe-miR-122/DOX group displayed enhanced cytotoxicity compared to DOX and Fe-miR-NC/DOX alone, potentially due to efficient miR122 release from the complex, leading to restored miR-122 expression within cells. This restoration promotes apoptosis in HepG2 cells, reducing chemotherapeutic resistance. We further conducted cytotoxicity assays in Huh-7 cells, with results mirroring those observed in HepG2 cells, thereby supporting the broader application of Fe-miR-122/DOX nanoparticles across various HCC cell lines. Moreover, Fe-miR-122/DOX nanoparticles exhibited lower toxicity towards normal liver
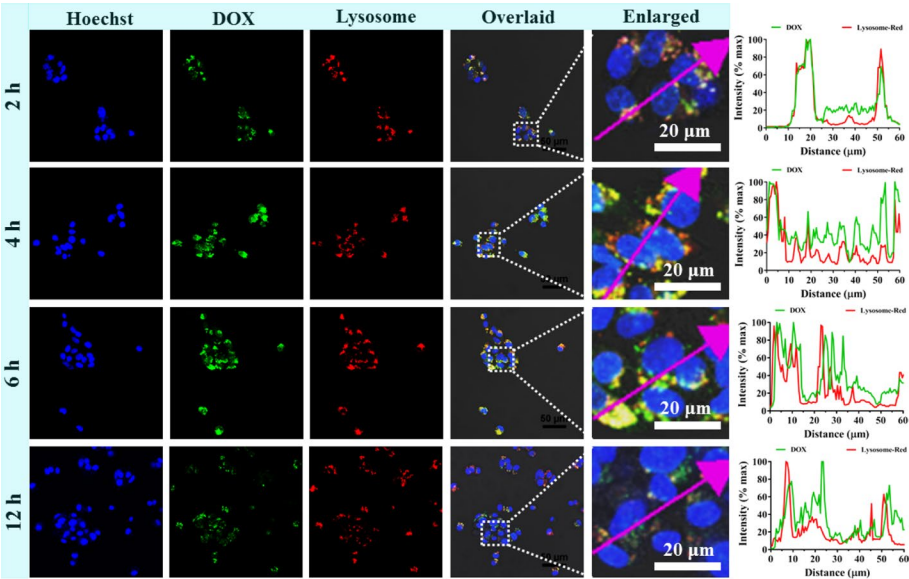
Fig. 4 a CLSM images of HepG2 cells treated with Fe-miR-122/DOX for different time. The nuclei and acidic compartments (endosomes and lysosomes) were stained with Hoechst (blue) and LysoTracker (red), respectively. Fluorescent intensity of DOX and lysosome (red) signals across 60-µm regions marked with arrows is shown in line plots
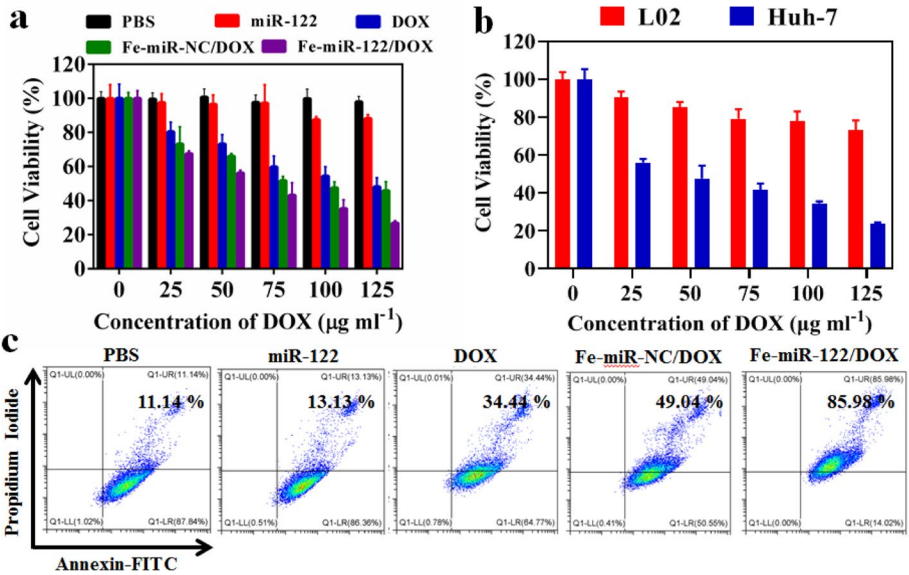

Fig. 5 **a** Cell viability of HepG2 cells with different treatments (n = 3). **b** Cell viability of Huh-7 and L02 cells with Fe-miR-122/DOX nanoparticles for 24 h (n = 3). **c** The apoptosis of HepG2 cells was treated with different samples by flow cytometric analysis

cells (L02 cells), likely due to the high endogenous expression of miR-122 in normal hepatocytes, which mitigates the impact of exogenous miR-122 (Fig. 5b). Additionally, the increased sensitivity of DOX to rapidly proliferating cancer cells and the specific release of nanoparticles within the tumor microenvironment contribute to this selective toxicity.

Lin *et al. Cancer Nanotechnology* (2024) 15:48

Page 11 of 15

To further explore how Fe-miR-122/DOX induces apoptosis to inhibit cell proliferation, we conducted assays using flow cytometry combined with FITC-labeled Annexin V/PI double staining (Fig. 5c). The results indicated apoptosis rates for cells treated with PBS, miR-122, DOX, Fe-miR-NC/DOX, and Fe-miR-122/DOX were 11.14%, 13.13%, 34.44%, 49.04%, and 85.98%, respectively. It was evidenced that the most significant pro-apoptotic effect was among the HepG2 cell populations, indicating the potent synergy between miR-122 and DOX in inducing apoptosis.

Mechanistic insights into Fe-miR-122/DOX-induced apoptosis and drug resistance reduction

According to previous research documented in references Fornari et al. (2009) and Xu et al. (2011), restoring miR-122 expression promotes apoptosis and reduces drug resistance. Specifically, miR-122 downregulates anti-apoptotic proteins such as Bcl-2 and the multidrug resistance gene (MDR1). In our study, we validated the expression levels of these miR-122-related downstream target proteins using Western blot analysis. Notably, to clearly demonstrate the effect of nanoparticle-delivered miR-122 and its synergistic action with DOX, we administered miR-122 directly rather than via transfection. Due to miR-122's inherent negative charge, it cannot easily penetrate the cell membrane without special treatment. However, once inside the cells via Fe-miR-122/DOX nanoparticles, miR-122 exerts its biological functions. As shown in Fig. 6a and additional file1: Fig. S15, the Fe-miR-122/DOX group exhibited reduced P-gp protein expression compared to the Fe-miR-NC/DOX group, indicating increased DOX accumulation within the cells. Further research revealed that miR-122 also caused a downregulation of Bcl-2 protein, leading to an increase in Caspase-3 protein expression. Quantitative analysis by Western blot further confirmed a significant reduction in P-gp and Bcl-2 protein levels, and an increase in caspase-3 protein expression in the Fe-miR-122/DOX group compared to the Fe-miR-NC/DOX group (Fig. 6b). This suggested that Fe-miR-122/DOX nanoparticles enhanced intracellular DOX accumulation by downregulating P-gp expression, and promoted apoptosis in HepG2 cells by downregulating Bcl-2 and upregulating caspase-3 expression.

Fe-miR-122/DOX nanoparticles exhibit unique advantages in HCC treatment, attributed to their efficient drug delivery capabilities and precise regulation of key protein expressions. cIAP1, a critical protein in the anti-apoptotic signaling pathway, is closely associated with tumor cell survival when overexpressed. Western blot analysis revealed that the Fe-miR-122/DOX group significantly inhibited cIAP1 expression (Fig. 6c and Addition file 1: Fig. S16), blocking the anti-apoptotic signaling pathway and reducing tumor cell viability. Additionally, PARP-1 is a widely distributed nuclear enzyme involved in recognizing and repairing DNA damage. Inhibiting PARP-1 prevents poly(ADP-ribosyl)ation (Hu et al. 2019; Rouleau et al. 2010), leading to DNA damage accumulation, enhancing chemosensitivity, and inducing apoptosis in drug-resistant cancer cells. Fe-miR-122/DOX disrupts the DNA repair mechanism by inhibiting PARP-1 expression (Fig. 6c and Addition file 1: Fig. S16), resulting in DNA damage accumulation and further weakening tumor cell viability, driving them towards apoptosis. Quantitative analysis showed that the Fe-miR-122/DOX group significantly lowered cIAP1 and PARP-1 expression, achieving a dual attack on tumor cells (Fig. 6d). These
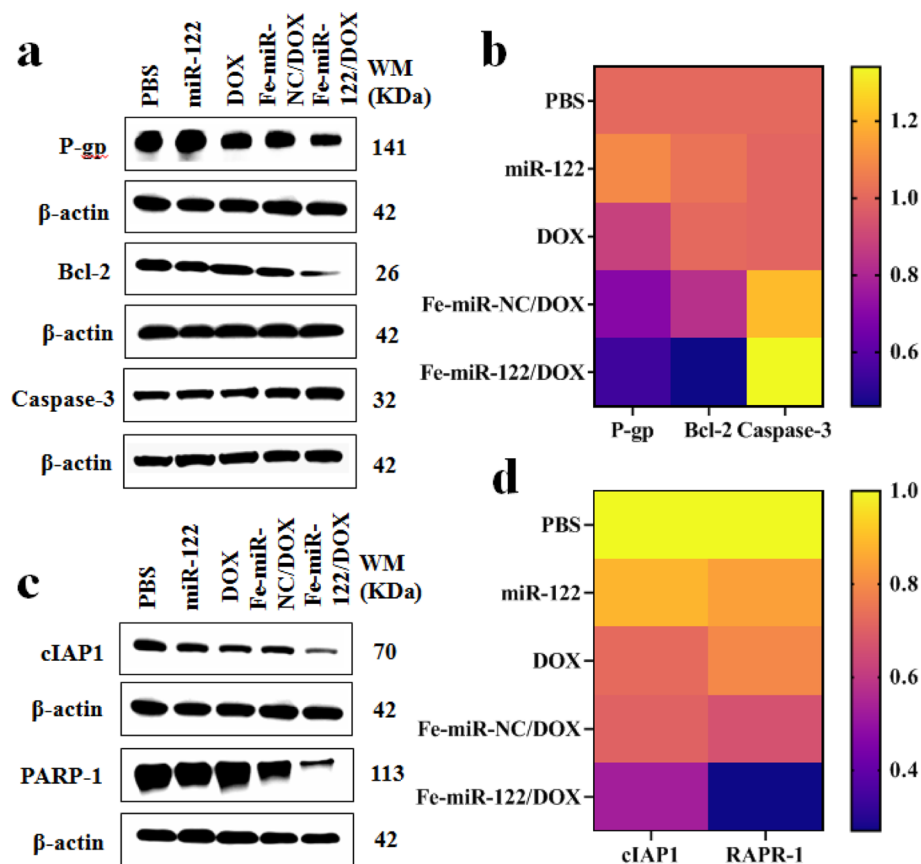
Lin *et al. Cancer Nanotechnology* (2024) 15:48

Page 12 of 15

Fig. 6 a Western blot analysis of P-gp, Bcl-2, and Caspase-3 protein expression levels in HepG2 cells under different treatment conditions. **b** Heatmap of the quantitative analysis of the Western blot results shown in Fig. 6a. **c** Western blot analysis of cIAP1 and PARP-1 protein expression levels in HepG2 cells under different treatment conditions. **d** Heatmap of the quantitative analysis of the Western blot results shown in Fig. 6c. Experimental setup: blank control group treated with PBS; miR-122 group at a concentration of 270 nmol L^{-1}; DOX group at a concentration of 50 μg mL^{-1}; Fe-miR-NC/DOX nanoparticles group with miR-NC at 270 nmol L^{-1} and DOX at 50 μg mL^{-1}; Fe-miR-122/DOX nanoparticles group with miR-122 at 270 nmol L^{-1} and DOX at 50 μg mL^{-1}. It should be noted that in SDS-PAGE gel electrophoresis analysis, P-gp and cIAP1 were run on the same gel, resulting in β-actin being present as a single band

findings not only validate the reliability of our experimental methods, but also reveal the underlying mechanisms by which Fe-miR-122/DOX nanoparticles overcome HCC cell resistance.

Therefore, the mechanism of action of Fe-miR-122/DOX nanoparticles can be elucidated as follows: first, Fe-miR-122/DOX delivers miR-122, downregulating the expression of the multidrug resistance gene P-gp, which leads to increased DOX accumulation. Concurrently, miR-122 downregulates the anti-apoptotic protein Bcl-2, resulting in the upregulation of the apoptosis-related protein Caspase-3, thereby promoting apoptosis in HepG2 cells. Second, the Fe-miR-122/DOX nanoparticles significantly inhibit the expression of cIAP1, a key protein in the anti-apoptotic signaling pathway, blocking the anti-apoptotic signal. Additionally, Fe-miR-122/DOX nanoparticles interfere with the DNA repair mechanism by inhibiting PARP-1 expression, leading to DNA damage accumulation and increased chemosensitivity. Finally, the nanoparticle delivery method overcomes the barrier of miR-122's direct entry into cells, ensuring efficient delivery

Lin *et al. Cancer Nanotechnology* (2024) 15:48

Page 13 of 15

and synergistic action. These mechanisms effectively overcome HCC cell resistance, significantly enhancing therapeutic outcomes and providing novel strategies for HCC treatment.

In vitro safety evaluation of Fe-miR-122/DOX nanoparticles via hemolysis assays

In vitro experiments demonstrated that Fe-miR-122/DOX nanoparticles can induce apoptosis and reduce drug resistance in HepG2 cells. Given the potential efficacy of Fe-miR-122/DOX nanoparticles in vivo, we evaluated their in vivo safety profile. Hemolysis assays are essential for assessing the biocompatibility of nanoparticles. In our experiment, fresh mouse blood was centrifuged and diluted with PBS (1:10 dilution). Subsequently, 0.2 mL of the diluted blood was incubated with 0.8 mL of varying concentrations of H_2O, PBS, and Fe-miR-122/DOX nanoparticles. H_2O served as the positive control, while PBS was the negative control. Under identical conditions, the absorbance of each sample was measured. The hemolysis rate was calculated using the following formula: Hemolysis rate $= [(A_{sample}-A_{PBS}) / (A_{H2O}-A_{PBS})] \times 100\%$. The results indicated that the hemolysis rate of Fe-miR-122/DOX nanoparticles at the highest concentration was approximately 2.82%, which is below the clinical threshold of 5%, suggesting good biocompatibility and no significant damage to red blood cells (Addition file 1: Fig. S17). Therefore, we conclude that Fe-miR-122/DOX nanoparticles exhibit good in vivo safety and hold promise for further in vivo studies.

Conclusions

In summary, our development of the co-delivery system Fe-miR-122/DOX represents a novel approach for combating HCC. Through the assembly of miR-122 with DOX and Fe^{II} iron, this system achieves synergistic therapy. Importantly, the Fe-miR-122/DOX system demonstrates the ability to modulate nanoparticle size based on reaction time. Confocal fluorescence imaging confirms its capability to facilitate synchronized drug release within cells, delivering miR-122 and DOX to the cytoplasm while escaping lysosomal degradation. After escape, the Fe-miR-122/DOX nanoparticles release miR-122, which reduces the expression of the efflux transporter P-gp, decreasing the efflux of DOX and concurrently downregulating the expression of the anti-apoptotic protein Bcl-2, leading to high expression of the apoptotic protein caspase-3 and effectively enhancing the chemotherapy effect, promoting the apoptosis of cancer cells. Moreover, Fe-miR-122/DOX effectively inhibits cIAPs-mediated anti-apoptotic signaling, downregulates PARP-1 expression, disrupts DNA repair, promotes DNA fragmentation accumulation, enhances caspase-3 activation, and triggers programmed cell death. This co-delivery system exhibits good biocompatibility and holds promise in reducing chemotherapy side effects and improving treatment specificity. With deeper understanding of the synergistic interaction between miR-122 and DOX, significant clinical benefits are anticipated, providing new therapeutic avenues for liver cancer patients.

Supplementary Information

The online version contains supplementary material available at https://doi.org/10.1186/s12645-024-00287-x.

Supplementary Material 1: Table S1. The information of DNA sequences in this work. Fig. S1. DLS measurement of Fe-miR122/DOX. Fig. S2. The TEM images of Fe-miR122/DOX at different reaction times. Fig. S3. DLS measurement

Lin *et al. Cancer Nanotechnology* (2024) 15:48

Page 14 of 15

of Fe-miR122/DOX at different reaction times. Fig. S4. UV–visible absorption spectroscopy of miR-122, DOX and Fe-miR122/DOX. Fig. S5. TEM images of Fe-miR122/DOX synthesized with different DOX: miR122 ratios: (a) 5:1, (b) 10:1, (c) 15:1 and (d) 20:1. Scale bar=500 nm. Fig. S6. Standard curves of fluorescence intensity versus concentration for miR122-Cy5 at 665 nm (a), DOX at 592 nm (b), and emission intensity versus concentration standard curve for ICP-MS quantification of Fe ions preparation concentration (c). miR122-Cy5 excitation at 635 nm, DOX excitation at 488 nm (n=3). Fig. S7. Fluorescence response of (a) miR122-Cy5 and (b) DOX. Fig. S8. The combination index (CI) of DOX and miR-122 at 10:1, 15:1, 20:1, 30:1 and 40:1 was evaluated by Chou–Talalay method. Fig. S9. The diameter of Fe-miR-122/DOX nanoparticles measured by DLS at different times (n=3). Fig. S10. TEM images (a), DLS measurement (b) and Zeta-potential analysis (c) of Fe-miR-NC/DOX at 60 min. Fig. S11. CLSM images of HepG2 cells treated with PBS, miR-122 and DOX for different time. Fig. S12. CLSM images of HepG2 cells treated with Fe-miR-NC/DOX for different time and fluorescent intensity of DOX and miR122-Cy5 signals across 60 µm regions marked with arrows is shown in line plots. Fig. S13. Pearson correlation coefficients between miR-122-Cy5 (red) and DOX (green) fluorescence signals at different time points. Fig. S14. Pearson correlation coefficients between lysosomal (red) and DOX (green) fluorescence signals at different time points. Fig. S15. Unaltered raw Western blot data displaying (a) P-gP, (b) Bcl-2, (c) Caspase-3 and their corresponding β-actin controls as depicted in Fig. 6a. Fig. S16 Unaltered raw Western blot data displaying (a) cIAP1, (b) PARP-1 and their corresponding β-actin controls as depicted in Fig. 6c. In the WB analysis, it is important to note that P-gp and cIAP1 were resolved on the same gel, which allowed for the β-actin to appear as a single band. Therefore, the β-actin images shown in Fig. S15a and Fig. S16a are derived from the same gel. Fig. S17. Hemolysis experiment determination of Fe-miR-122/DOX hemolysis of red blood cells in whole blood effect.

References

Agirre M, Zarate J, Ojeda E, Puras G, Desbrieres J, Pedraz J (2014) Low molecular weight chitosan (LMWC)-based polyplexes for pDNA delivery: from bench to bedside. Polymers 6(6):1727–1755. https://doi.org/10.3390/polym6061727

Bracken CP, Scott HS, Goodall GJ (2016) A network-biology perspective of microRNA function and dysfunction in cancer. Nat Rev Genet 17(12):719–732. https://doi.org/10.1038/nrg.2016.134

Bray F, Ferlay J, Soerjomataram I, Siegel RL, Torre LA, Jemal A (2018) Global cancer statistics 2018: GLOBOCAN estimates of incidence and mortality worldwide for 36 cancers in 185 countries. CA Cancer J Clin 68(6):394–424. https://doi.org/10.3322/caac.21492

Cao F, Yin L-X (2019) miR-122 enhances sensitivity of hepatocellular carcinoma to oxaliplatin via inhibiting MDR1 by targeting Wnt/β-catenin pathway. Exp Mole Pathol 106:34–43. https://doi.org/10.1016/j.yexmp.2018.10.009

Fornari F, Gramantieri L, Giovannini C, Veronese A, Ferracin M, Sabbioni S et al (2009) MiR-122/cyclin G1 interaction modulates p53 activity and affects doxorubicin sensitivity of human hepatocarcinoma cells. Cancer Res 69(14):5761–5767. https://doi.org/10.1158/0008-5472.can-08-4797

Hu K, Wu W, Li Y, Lin L, Chen D, Yan H et al (2019) Poly (ADP-ribosyl) ation of BRD7 by PARP1 confers resistance to DNA-damaging chemotherapeutic agents. EMBO Rep 20(5):e46166. https://doi.org/10.15252/embr.201846166

Lee D, Jang M-K, Seo JH, Ryu SH, Kim JA, Chung Y-H (2018) ARD1/NAA10 in hepatocellular carcinoma: pathways and clinical implications. Exp Mol Med 50(7):1–12. https://doi.org/10.1038/s12276-018-0106-1

Li M, Wang C, Di Z, Li H, Zhang J, Xue W et al (2018) Engineering multifunctional DNA hybrid nanospheres through coordination-driven self-assembly. Angew Chem Int Edit 58(5):1350–1354. https://doi.org/10.1002/anie.201810735

Li J, Li Y, Pan L, Pan W, Li N, Tang B (2022) Spherical nucleic acids-based biosensors for cancer biomarkers detection. TrAC Trend Anal Chem 157:116807. https://doi.org/10.1016/j.trac.2022.116807

Lin *et al. Cancer Nanotechnology* (2024) 15:48

Page 15 of 15

Li S, Chen S, Dong Z, Song X, Li X, Huang Z et al (2023) Concurrent silencing of TBCE and drug delivery to overcome platinum-based resistance in liver cancer. Acta Pharm Sin B 13(3):967–981. https://doi.org/10.1016/j.apsb.2022.03.003

Mendes BB, Conniot J, Avital A, Yao D, Jiang X, Zhou X, S, et al (2022) Nanodelivery of nucleic acids. Nat Rev Method Prime. https://doi.org/10.1038/s43586-022-00104-y

Nakao K, Miyaaki H, Ichikawa T (2014) Antitumor function of microRNA-122 against hepatocellular carcinoma. J Gastroenterol 49(4):589–593. https://doi.org/10.1007/s00535-014-0932-4

Rouleau M, Patel A, Hendzel MJ, Kaufmann SH, Poirier GG (2010) PARP inhibition: PARP1 and beyond. Nat Rev Genet 10(4):293–301. https://doi.org/10.1038/nrc2812

Rupaimoole R, Slack FJ (2017) MicroRNA therapeutics: towards a new era for the management of cancer and other diseases. Nat Rev Drug Discov 16(3):203–222. https://doi.org/10.1038/nrd.2016.246

Takai Takamatsu R, Okano A, Yamakawa G, Mizukoshi K, Obayashi H, Ohana M (2019) Impact of an ultrasound-guided radiofrequency ablation training program on the outcomes in patients with hepatocellular carcinoma. Diagn Inter Imag 100(12):771–780. https://doi.org/10.1016/j.diii.2019.08.004

Vogel A, Meyer T, Sapisochin G, Salem R, Saborowski A (2022) Hepatocellular carcinoma. Lancet 400(10360):1345–1362. https://doi.org/10.1016/s0140-6736(22)01200-4

Wang S, McGuirk CM, d'Aquino A, Mason JA, Mirkin CA (2018) Metal-organic framework nanoparticles. Adv Mater 30(37):e1800202. https://doi.org/10.1002/adma.201800202

Wang R, Yin C, Liu C, Sun Y, Xiao P, Li J, Yang S, Wu W, Jiang X (2021a) Phenylboronic acid modification augments the lysosome escape and antitumor efficacy of a cylindrical polymer brush-based prodrug. J Am Chem Soc 143(49):20927–20938. https://doi.org/10.1021/jacs.1c09741

Wang X, Chen Y, Dong K, Ma Y, Jin Q, Yin S et al (2021b) Effects of FER1L4-miR-106a-5p/miR-372-5p-E2F1 regulatory axis on drug resistance in liver cancer chemotherapy. Mol Ther-Nucl Acids 24:449–461. https://doi.org/10.1016/j.omtn.2021.02.006

Xiong Q, Bai Y, Shi R, Wang J, Xu W, Zhang M et al (2021a) Preferentially released miR-122 from cyclodextrin-based star copolymer nanoparticle enhances hepatoma chemotherapy by apoptosis induction and cytotoxics efflux inhibition. Bioact Mater 6(11):3744–3755. https://doi.org/10.1016/j.bioactmat.2021.03.026

Xiong Q, Bai Y, Shi R, Wang J, Xu W, Zhang M et al (2021b) Preferentially released miR-122 from cyclodextrin-based star copolymer nanoparticle enhances hepatoma chemotherapy by apoptosis induction and cytotoxics efflux inhibition. Bioact Mater 6(11):3744–3755. https://doi.org/10.1016/j.bioactmat.2021.03.026

Xu Y, Xia F, Ma L, Shan J, Shen J, Yang Z et al (2011) MicroRNA-122 sensitizes HCC cancer cells to adriamycin and vincristine through modulating expression of MDR and inducing cell cycle arrest. Cancer Lett 310(2):160–169. https://doi.org/10.1016/j.canlet.2011.06.027

Xu J, Zhu X, Wu L, Yang R, Yang Z, Wang Q et al (2012) MicroRNA-122 suppresses cell proliferation and induces cell apoptosis in hepatocellular carcinoma by directly targeting Wnt/β-catenin pathway. Liver Int 32(5):752–760. https://doi.org/10.1111/j.1478-3231.2011.02750.x

Yarchoan M, Agarwal P, Villanueva A, Rao S, Dawson LA, Karasic T et al (2019) Recent developments and therapeutic strategies against hepatocellular carcinoma. Cancer Res 79(17):4326–4330. https://doi.org/10.1158/0008-5472.can-19-0803

Yingchoncharoen P, Kalinowski DS, Richardson DR, Barker EL (2016) Lipid-based drug delivery systems in cancer therapy: what is available and what is yet to come. Pharmacol Rev 68(3):701–787. https://doi.org/10.1124/pr.115.012070

Zou Z, He L, Deng X, Wang H, Huang Z, Xue Q et al (2021) Zn^{2+}-coordination-driven RNA assembly with retained integrity and biological functions. Angew Chem Int Edit 60(42):22970–22976. https://doi.org/10.1002/anie.202110404

Publisher's Note